Available online at www.sciencedirect.com
ScienceDirect
Trans. Nonferrous Met. Soc. China 33(2023) 1460−1471
Transactions of Nonferrous Metals Society of China
www.tnmsc.cn

Stress analysis and microstructure evolution of Cu/Al composite plate during corrugated rolling

Yan-xiao LIU[1], Yuan-ming LIU[1,2,3], Zhen-hua WANG[1,2,3], Yan-ping LIU[1], Tao WANG[1,2,3], Qing-xue HUANG[1,2,3]

1. College of Mechanical and Vehicle Engineering, Taiyuan University of Technology, Taiyuan 030024, China;
2. Engineering Research Center of Advanced Metal Composites Forming Technology and Equipment, Ministry of Education, Taiyuan University of Technology, Taiyuan 030024, China;
3. TYUT-UOW Joint Research Center, Taiyuan University of Technology, Taiyuan 030024, China

Received 19 December 2021; accepted 9 March 2022

Abstract: A 3D finite element model was developed. The accuracy of the model was verified through a rolling experiment in which the reduction rate of the plate was 50%. The metal flow law in the rolling process was analyzed from the perspective of time during the whole corrugated rolling process. The deformation experienced by all metal particles is divided into two periods: the filling period and the extension period. The stress change is complex during the filling period, but the stress change trend is approximate during the extension period. The stress state of characteristic positions is two tensile stresses and one compressive stress when the plate starts to deform, which was analyzed by the Lode angle parameter and triaxiality parameter. The microstructure evolution of the Cu plate was analyzed using electron backscatter diffraction (EBSD) technology. Compared with the initial plate, grain refinement occurs at each characteristic position of the Cu plate. There is a phenomenon of grain growth at the trough of the Cu plate after refinement due to the adiabatic temperature increase caused by severe plastic deformation.

Key words: Cu/Al composite plate; corrugated rolling; deformation behavior; stress analysis; microstructure evolution

1 Introduction

With the increasing demand for plate properties in modern industry, it is urgent to study bimetallic composites, which can combine the advantageous properties of two metals and can significantly enhance the strength or corrosion resistance of the material [1,2]. The Cu/Al composite plate has not only good electrical and thermal conductivity of Cu but also light mass and low price advantages of Al. Therefore, the composite plates are widely used in various fields, such as electronics, power, metallurgical equipment, machinery, automobiles, energy and household appliances [3]. The traditional composite plate manufacturing technology includes the explosive welding [4], cold drawing [5], friction welding [6] and roll bonding [7]. Roll bonding is widely used because of its simple process, convenient operation and low energy consumption.

CHANG et al [8] studied the influence of asymmetrical roll bonding on Cu/Al composite plates. The bond strength and tensile strength were found to be higher when the rotation speed ratio was 1.3. The intermetallic compounds at the interface of the Cu/Al composite plate were also analyzed. Al_2Cu was formed first, and then Al_4Cu_9 was generated between Al_2Cu and Cu. After that, AlCu was generated between the Al_2Cu and Al_4Cu_9 [9]. Through tensile tests of laminated composites produced by asymmetrical roll bonding with different strain rates, the strength and elongation can be found to increase with increasing

Corresponding author: Yuan-ming LIU, Tel/Fax: +86-351-6014008, E-mail: liuyuanming@tyut.edu.cn
DOI: 10.1016/S1003-6326(23)66196-5

the strain rate [10]. The microstructure and texture evolution of a cumulatively rolled Mg/Nb composite plate was analyzed by using diffraction methods and polycrystal modelling. Annealing treatment was shown to change the texture of Mg alloys but did not change the texture of Nb [11]. In cold rolling, the greater the thickness reduction is, the greater the critical strain of the onset of plastic instability is [12]. Necking began to occur, and the interface was wavy when the reduction was 12.5%.

To further analyze the rolling process of composite plates, many scholars used finite element software to simulate the rolling process. CHEN [13] established a Cu/Al composite plate model with internal defects to explore the evolution of the correlation between the upper/lower voids with different processes. HUANG et al [14] used the velocity field to analyze the cold rolling bonding process. The bonding strength was reduced with increasing roller circumferential velocity, and the synchronicity of metal flow on the bonding surface decreased. DYJA et al [15] proposed a three-dimensional rigid-plastic model to analyze the deformation of a bimetallic material and research the metal flow during the rolling process of bimetallic rods. PAN et al [16] analyzed the asymmetrical cold and hot bond rolling of a two-layered unbounded clad sheet and found that a smaller shear yield stress ratio was beneficial to composite plate bonding. LU et al [17] established a three-dimensional elastic-plastic model of Ti/Al composite sheets, which can be used to predict the forming limit curve with different geometries or stacking proportions. MOHEBBI and AKBARZADEH [18] established the cryorolled models of different reductions to verify the reliability of finite element method (FEM) and obtained the deformation conditions of the specimen at different incremental rolling passes through FEM.

Recently, a new corrugated rolling technology for the composite plates has attracted wide attention due to good mechanical properties of the product [19]. WANG et al [20,21] found that the preparation of Mg/Al composite plates by the corrugated rolling process promoted grain refinement at the bonding interface, improved the interface bonding strength, reduced the residual stress and improved the shape of the plate. Research on corrugated rolled composite plates has mainly focused on the mechanical properties of rolled plates. However, the metal flow law and microstructure evolution characteristics in the rolling process of composite plates have rarely been clarified. The surface of the composite plate prepared by the corrugated roller is corrugated. The difference from traditional flat rolling is that the change process experienced by each position is different. Therefore, the changing process of different positions in a waveform is of great significance to enhance the advantage of the corrugated rolling process. In this study, a three-dimensional finite element model was developed for the corrugated rolling of Cu/Al composite plates. The stress change and metal flow in the deformation process of composite plates were analyzed by FEM. Combining electron backscatter diffraction (EBSD), the microstructure evolution was also analyzed.

2 Experimental

2.1 Materials and processing

In this work, 5052Al plates with a size of 150 mm × 50 mm × 4 mm and T2 Cu plates with a size of 150 mm × 50 mm × 1 mm were used. The chemical composition of the materials is shown in Table 1.

Table 1 Chemical composition of experimental materials (wt.%)

Alloy	Cu	Al	Fe	Cr	Mg	Zn	Si
T2Cu	Bal.	−	0.0031	−	−	−	−
5052Al	0.1	Bal.	0.4	0.15−0.35	2.2−2.8	0.1	0.25

Before the experiment, the bonded surface of the plate was polished using a grinder to remove the oxide layer. Then, the surface was wiped with alcohol to remove oil pollution and metal debris, as shown in Fig. 1(a). After surface treatment, the head and tail of the plate were bonded with Al wire. The combination was rolled in a two-roller mill with a dynamic signal test and analysis system (Model DH5922D). The upper roller was corrugated with a sine curve feature, in which the equivalent diameter was 150 mm, the number of waves was 100, the amplitude was 0.55 mm, and the cycle period was 0.0628 s. The lower roller was a flat roller with a diameter of 150 mm. The Cu plate was in contact

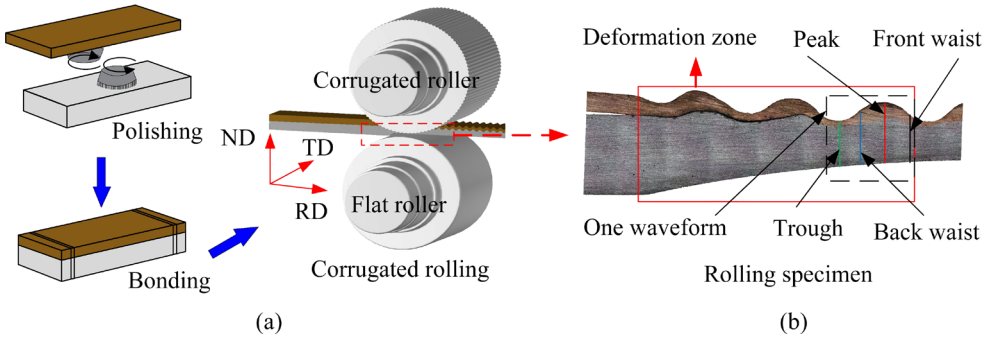

Fig. 1 Schematic diagrams of corrugated rolling (a) and rolling specimen (b)

with the corrugated roller, and the Al plate was in contact with the flat roller. The experiment was carried out at room temperature, and the reduction rate was 50%. By stopping the roller suddenly during the rolling process, the rolling block specimen was obtained, as shown in Fig. 1(b). The rolling direction is defined as RD, the normal direction is ND, and the transverse direction is TD.

The rolling block specimen containing the rolling deformation zone was cut by wire electrical discharge machining. The peak and trough positions of the upper surface were not in one-to-one correspondence with those of the bonding interface, as shown in Fig. 1(b). To facilitate the analysis, four characteristic positions (front waist, peak, back waist and trough) of the bonding interface and the lower surface of the Al plate were determined based on the upper surface of the rolled Cu plate in a waveform around the exit. The RD–ND surface of the sample was mechanically ground by SiC sandpaper (180#, 400#, 800#, 1200#, 1500#, and 2000#). Then, the surface was mechanically polished with a 3 mm diamond suspension and put into a vibrating polishing machine for 3 h. Subsequently, the sample was electrolyzed with a methanol solution containing 30% nitric acid at −30 °C and 12 V for 10 s and observed through EBSD.

2.2 Rolling model establishment and verification

2.2.1 Model establishment

A three-dimensional finite element rolling model is established, as shown in Fig. 2, and is divided into the roller and the composite plate. Since the roller deformation is very small compared to the composite plate, the roller is set to be a rigid body. Assuming that the Cu plate and Al plate are isotropic elastic-plastic materials, the Cu plate–Al plate, Cu plate–roller and Al plate–roller contact conditions are set to be face-to-face penalty contact. Due to the symmetry in the width direction, only a half model is established to save calculation time. Therefore, the size of the Cu plate is 50 mm × 25 mm × 1 mm, and the size of the Al plate is 50 mm × 25 mm × 4 mm. The angular velocity of the roller is 1.3 rad/s, and the plate initial speed is 60 mm/s, which are the same as the actual rolling experiment. The grid adopts solid element C3D8R, and the mesh size is 0.2 mm × 0.2 mm × 0.2 mm.

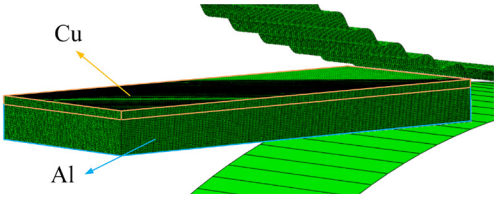

Fig. 2 Finite element model of corrugated rolling

2.2.2 Model verification

The rolling force of the simulation is obtained and compared with the actual rolling force. Because the plate length in the FEM model is 1/3 of the actual length, the duration of the simulation force is 1/3 of the actual duration, as shown in Fig. 3. The actual rolling force is between 304.87 and 329.24 kN, and the simulated rolling force is between 309.55 and 348.79 kN. The maximum error between the actual and simulated rolling force is less than 8%.

As shown in Fig. 4, the thickness of the composite plate and the thickness of the Cu plate are extracted in the FEM and experiment. The thickness of the rolled composite plate is slightly larger than that of the simulation because the roller is a rigid body in the FEM. In the actual rolling process, the roller is an elastoplastic body, and elastic deformation occurs. The thicknesses of the

Cu plate in the simulation and experiment are roughly the same. The average height error is less than 2%. Therefore, the finite element simulation results are reliable.

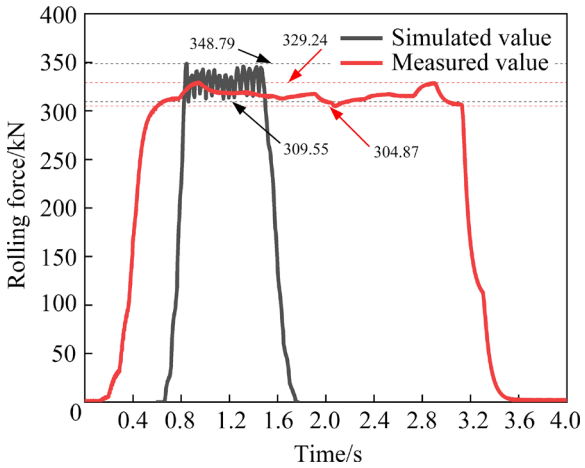

Fig. 3 Comparison of simulated and measured rolling force

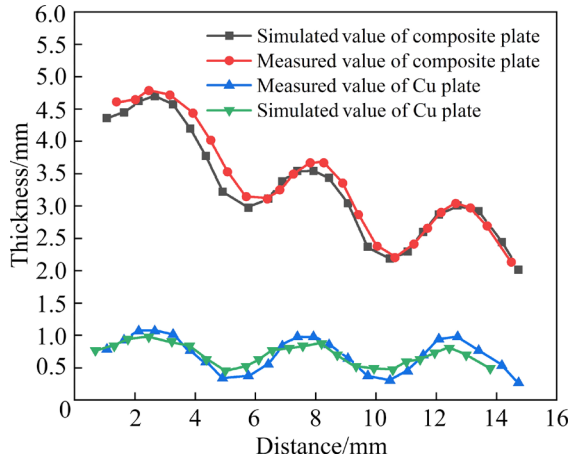

Fig. 4 Comparison of simulated and measured thickness

3 Results and discussion

3.1 Stress variation characteristics

In the rolling process, stress and strain are the main factors of composite plate bonding, and they significantly influence the deformation and warpage of the composite plate [22,23]. The corrugated rolling process can be regarded as the process in which one after another waveform of the metal passes through the rolling deformation zone. In the stable rolling stage, the metal of each waveform in the deformation zone is deformed in the same way. Therefore, the metal deformation in the whole corrugated rolling process can be obtained by researching the deformation of one waveform in the deformation zone. The waveform near the exit side (as shown in Fig. 1(b)) of the deformation zone is selected as the research object.

Figure 5(a) shows the normal stress at the characteristic positions on the upper surface of the Cu plate. The composite plate starts to move in the rolling direction when the time is 0, and the observation waveform does not touch the roller until 0.25 s. The stress at the peak begins to increase at 0.25 s and reaches the peak value at 0.267 s. The stress at the front waist reaches a peak value at the same time. Then, the stresses of the peak and front waist both begin to decrease. At 0.30 s, the stress direction changes at the front waist and reaches a maximum at 0.325 s. Meanwhile, the stress at the trough begins to increase. The stresses at the back waist and front waist begin to increase at 0.325 and 0.333 s, respectively. After that, the stress of each position increases gradually. The maximum stress is larger at the trough than that at other positions, and the maximum stress at the front waist is significantly smaller than that at other positions.

Figure 5(b) shows the normal stress at the characteristic positions on the lower surface of the Cu plate. The stress at the peak and front waist increases due to contact with the Al plate and then decreases. However, the stress at the back waist begins to increase at 0.3 s. The stress at the trough begins to increase last. When reaching 0.342 s, the stress at the peak and back waist increases again. Subsequently, the stress at each position first increases and then decreases again. In particular, the stress at the trough suddenly increases at 0.43 s and then reaches the peak value. The maximum stresses at the trough and back waist are larger than those at the peak and front waist. Figure 5(c) shows the stress at the characteristic positions on the lower surface of the Al plate. The four characteristic positions are in contact with the flat roller in sequential order (front waist, peak, back waist and trough), and their changing trends are similar.

Figure 5(d) shows the equivalent strain at each characteristic position of the lower surface of the Cu plate. The equivalent strain continues to grow as the rolling experiment proceeds, but there is a sharp rise marked by the green frame in the trough. The sudden increase of equivalent strain at the trough is due to the sharp increase in the stress, which is caused by the corrugated roller shape, as shown in Fig. 5(b).

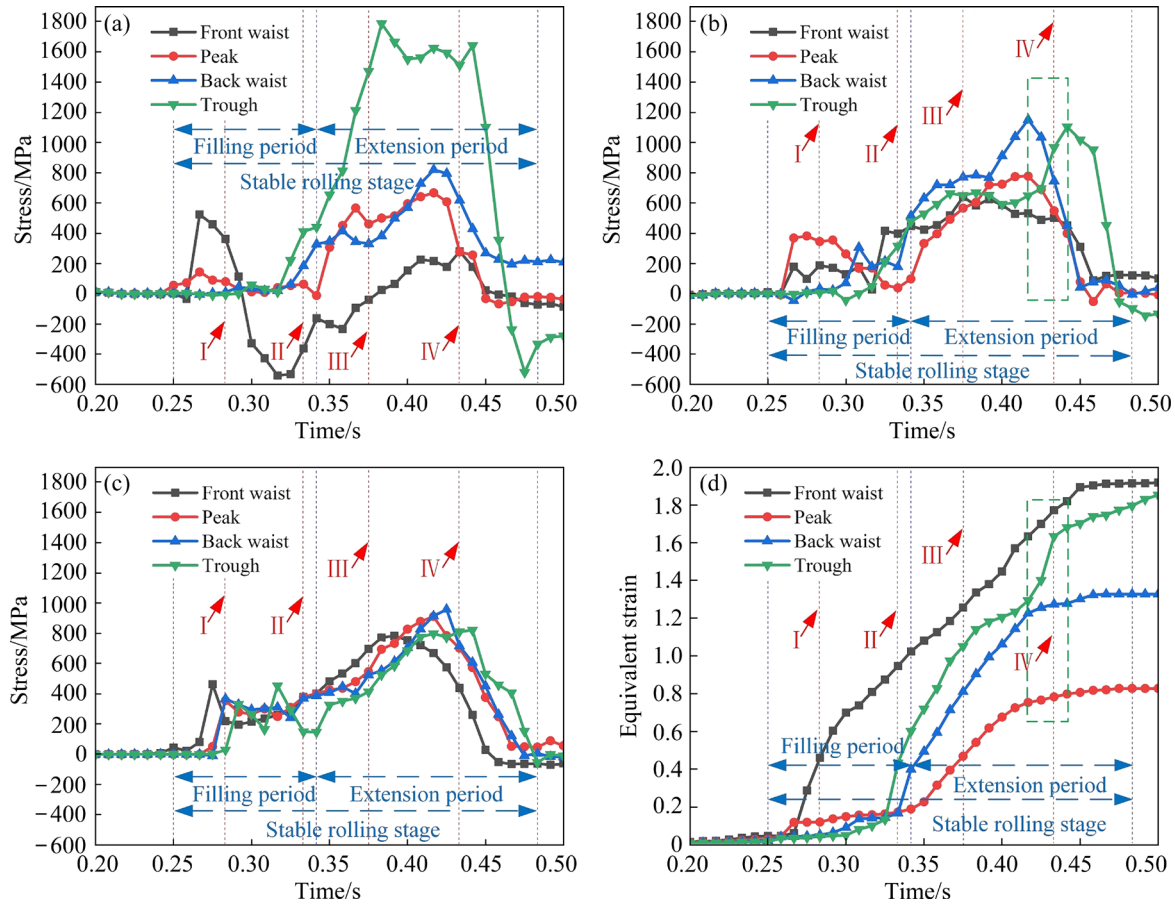

Fig. 5 Stress distribution of upper surface of Cu plate (a), lower surface of Cu plate (b), lower surface of Al plate (c), and equivalent strain on lower surface of Cu plate (d)

3.2 Metal flow of rolling process

Since the deformation experienced by each waveform is the same, the deformation law of the entire composite plate during the rolling process can be obtained by researching the change of one waveform with time. The region of the selected waveform is determined as Region IV. The characteristic positions on the selected waveform are marked in the rolling block specimen according to the FEM, and the corresponding time is 0.433 s, as shown in Fig. 6(a). The composite plate is moved to the rolling entrance side in the FEM by setting the analysis step time back until the selected waveform just leaves Region IV. At this time, the analysis step time is 0.375 s. The region where the selected waveform is located is defined as Region III, and the characteristic points are marked on the rolling block specimen according to the FEM. The composite board continues to move to the entrance side, and Regions II and I are defined by the same method in turn, as shown in Fig. 6(b), and the corresponding time is 0.333 and 0.283 s, respectively. Different colours are used to indicate different characteristic positions. Points a, b, c and d are the characteristic positions on the lower surface of the Cu plate, Points e, f, g and h are the characteristic positions on the upper surface of the Cu plate, and Points i, j, k and l are the characteristic positions on the lower surface of the Al plate, as shown in Fig. 6(c). Subscripts are used to indicate the region number. The process of the exit side waveform changing with time in the deformation zone can be more easily understood through the characteristic positions at these moments.

The metal flow on the upper surface of the Cu plate is analyzed by combining Fig. 5(a) with Fig. 6(c). The stress of the peak increases first at 0.25 s, as shown in Fig. 5(a). Therefore, the peak first contacts the corrugated roller. When the plate is extended under the action of extrusion by the roller, the stress of the peak decreases, and the metal flows to the entrance side. At the same time, the front waist contacts the corrugated roller, and its

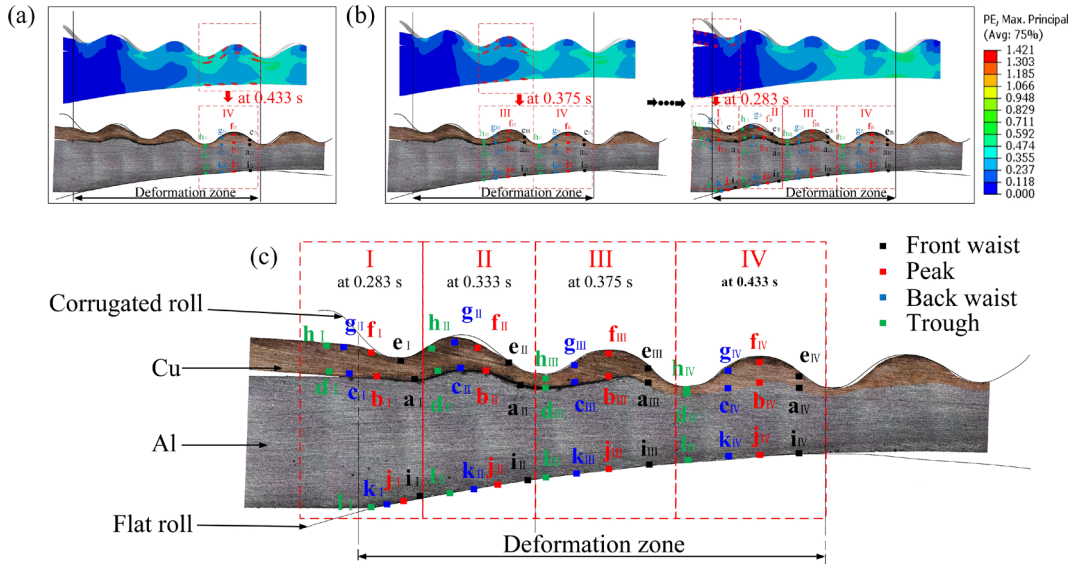

Fig. 6 Corresponding FEM and experiment in Region IV (a), corresponding process in Regions III, II and I (b), and schematic diagram of characteristic position distribution (c)

stress begins to rise. At 0.283 s, the front waist moves to Position e_I in Fig. 6(c), and Position f_I is about to leave the roller. Therefore, the stress at the peak disappears at 0.291 s. After that, the extrusion effect of the roller on the metal at the trough position of Region II makes Position e_I move to Position f_I. The stress direction changes at the front waist because the peak of the corrugated roller near the front waist squeezes the metal. Subsequently, the trough is in contact with the corrugated roller and moves to the exit side relative to the corrugated roller as the stress increases until it reaches Position h_{II} (0.333 s). In the following process, the back waist (g), peak (f) and front waist (e) contact the roller in turn, and their stresses first increase and then decrease within the time corresponding to Regions II, III and IV, respectively. The maximum stress is greater at the trough position than that at the other positions because the actual reduction rate at the trough is the largest.

The metal flow on the lower surface of the Cu plate is analyzed using the results in Fig. 5(b) and Fig. 6(c). At 0.283 s (corresponding to Region I), peak b_I and front waist a_I are first subjected to compressive stress. As the front waist and peak move to the entrance side and fill the corrugated roller trough, the stress decreases. Through the increase in stress, as seen in Fig. 5(b), the back waist and trough are, in turn, in contact with the Al plate. At 0.333 s (corresponding to Region II), the Cu and Al plates are in close contact, and the stress at each position increases. After that, the stress change at each position is similar to that of the traditional flat rolling process, in which the stress increases to the maximum value and then decreases at the end of rolling [24]. However, due to the corrugated roller shape, the back waist and trough have greater stress at 0.433 s (corresponding to Region IV).

The characteristic positions of the lower Al surface enter the rolling deformation zone in turn, corresponding to the stress increase, as shown in Fig. 5(c). When the upper surface of the Cu plate is separated from the corrugated roller at 0.283 s (corresponding to Region I), the stress at each position on the lower surface of the Al plate begins to decrease. Subsequently, the change process is similar to that of the lower surface of the Cu plate.

In summary, the metal of the Cu plate moves to the entrance side at 0.283 s (corresponding to Region I), and the flow rate of the upper surface is faster than that of the lower surface. At 0.333 s (corresponding to Region II), two adjacent peaks of the corrugated roller (Positions e_I and h_{II}) are in contact with the Cu plate and produce a pinning effect. The metal flow of the Cu plate towards the exit side is hindered. The metal in Region II fills the trough of the corrugated roller. Because the pinning effect on the upper surface is stronger than that on the lower surface, the filling speed of the upper surface of the Cu plate is faster than that of the lower surface. In other words, the upper surface

metal of the Cu plate moves to the exit side relative to the lower surface metal. The characteristic positions of the upper and lower surfaces of the Cu plate are relatively unchanged until 0.375 s (corresponding to Region III). From 0.375 s (corresponding to Region III) to 0.433 s (corresponding to Region IV), the Cu plate only produces a small reduction. The thickness change of the composite plate mainly comes from the thinning of the Al plate.

According to the stress change and metal flow, the deformation experienced by all metal particles in the corrugated rolling process is divided into two periods: the filling period and the extension period. During the filling period, the deformed Cu plate fills the trough of the corrugated roller, and the stress change is complicated. The Cu plate fully contacts the corrugated roller during the extension period, and the stress change trend of each characteristic position is approximate.

3.3 Cross shear phenomenon

The cross shear zone is formed when the shear stress directions of the upper and lower surfaces in the deformation zone are opposite [3]. The cross shear action not only promotes the fracture of the interface metals but also makes the interface between the two metals have a stronger relative shear and rubbing effect [22]. Each characteristic position undergoes cross shear action in the extension period, as shown in Fig. 7. The metal crack caused by the cross shear action promotes the bonding of the composite plate. The front waist is first subjected to cross shear action, and then the trough begins to undergo cross shear action. The back waist is subjected to cross shear action at approximately 0.433 s (corresponding to Region IV), and the peak undergoes cross shear action when the rolling ends. However, the duration of the cross shear action at the front waist and trough is longer than that at the peak and back waist. This is also one of the reasons that the equivalent strain is larger at the front waist and trough than that at the other two characteristic positions.

3.4 Stress state evolution

The stress state in the rolling process is always judged using the Lode angle parameter and the triaxiality parameter. BAI and WIERZBICKI [25] presented a method to express the stress state in the

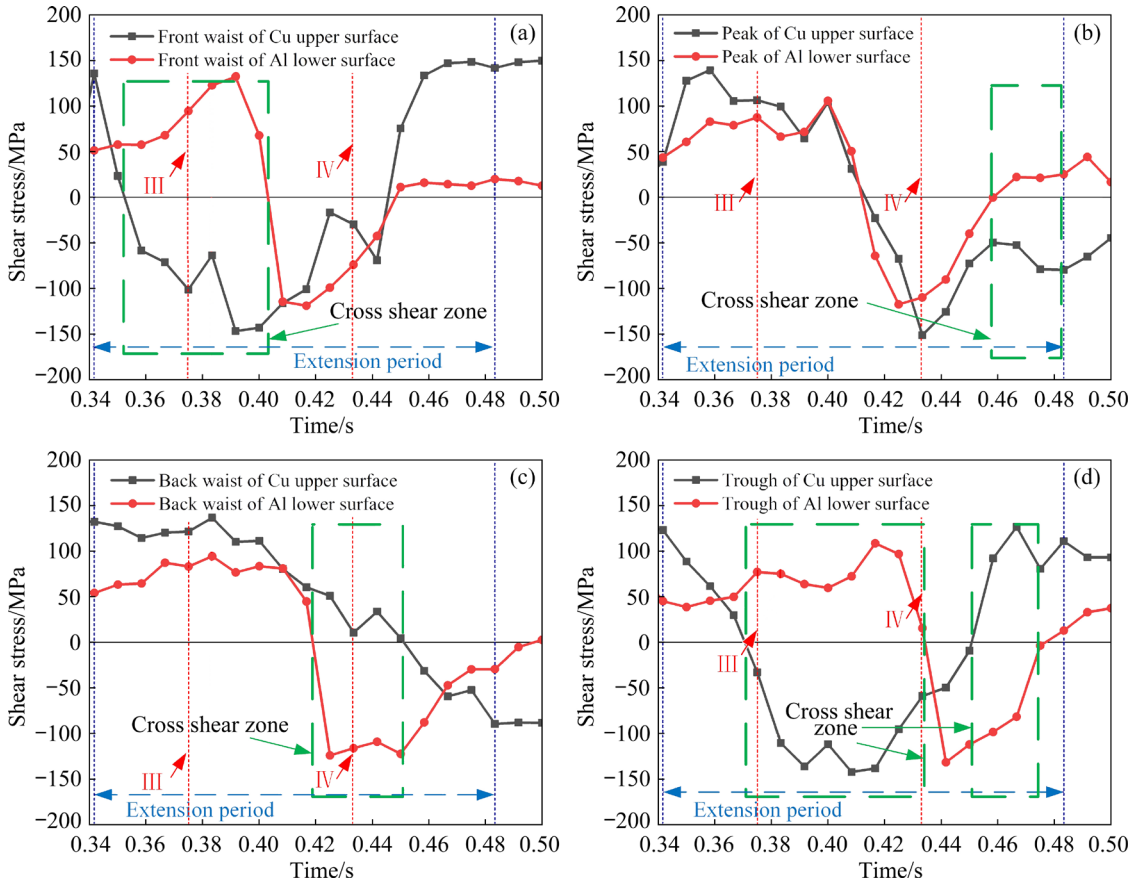

Fig. 7 Shear stress at characteristic positions: (a) Front waist; (b) Peak; (c) Back waist; (d) Trough

η (triaxiality parameter) and $\bar{\theta}$ (Lode angle parameter) plane, as shown in Fig. 8(a). WANG [26] explained the stress state of each area. Area 1 is subjected to triaxial tensile stresses, as indicated by the green dots. Area 2 is subjected to two tensile stresses and one compressive stress, as indicated by the blue dots. Area 3 is subjected to two compressive stresses and one tensile stress, as indicated by the red dots. Area 4 is subjected to triaxial compressive stresses, as indicated by the black dots. Through the above normal and shear stress analysis, the complex changes in the stress are mainly on the Cu plate side of the corrugated rolling. Therefore, the stress state of the Cu plate side is analyzed. According to the FEM results, η can be obtained from Eq. (1):

$$\eta = \sigma_m / \bar{\sigma} \tag{1}$$

where σ_m is the average value of the three normal stresses (σ_1, σ_2 and σ_3) and $\sigma_m=(\sigma_1+\sigma_2+\sigma_3)/3$, and $\bar{\sigma}$ is the equivalent stress and can be obtained from Eq. (2):

$$\bar{\sigma} = \{\frac{1}{2}[(\sigma_1-\sigma_2)^2+(\sigma_3-\sigma_2)^2+(\sigma_1-\sigma_3)^2+ 6(\tau_{12}^2+\tau_{23}^2+\tau_{31}^2)]\}^{1/2} \tag{2}$$

where τ_{12}, τ_{23} and τ_{31} are the three shear stresses, respectively.

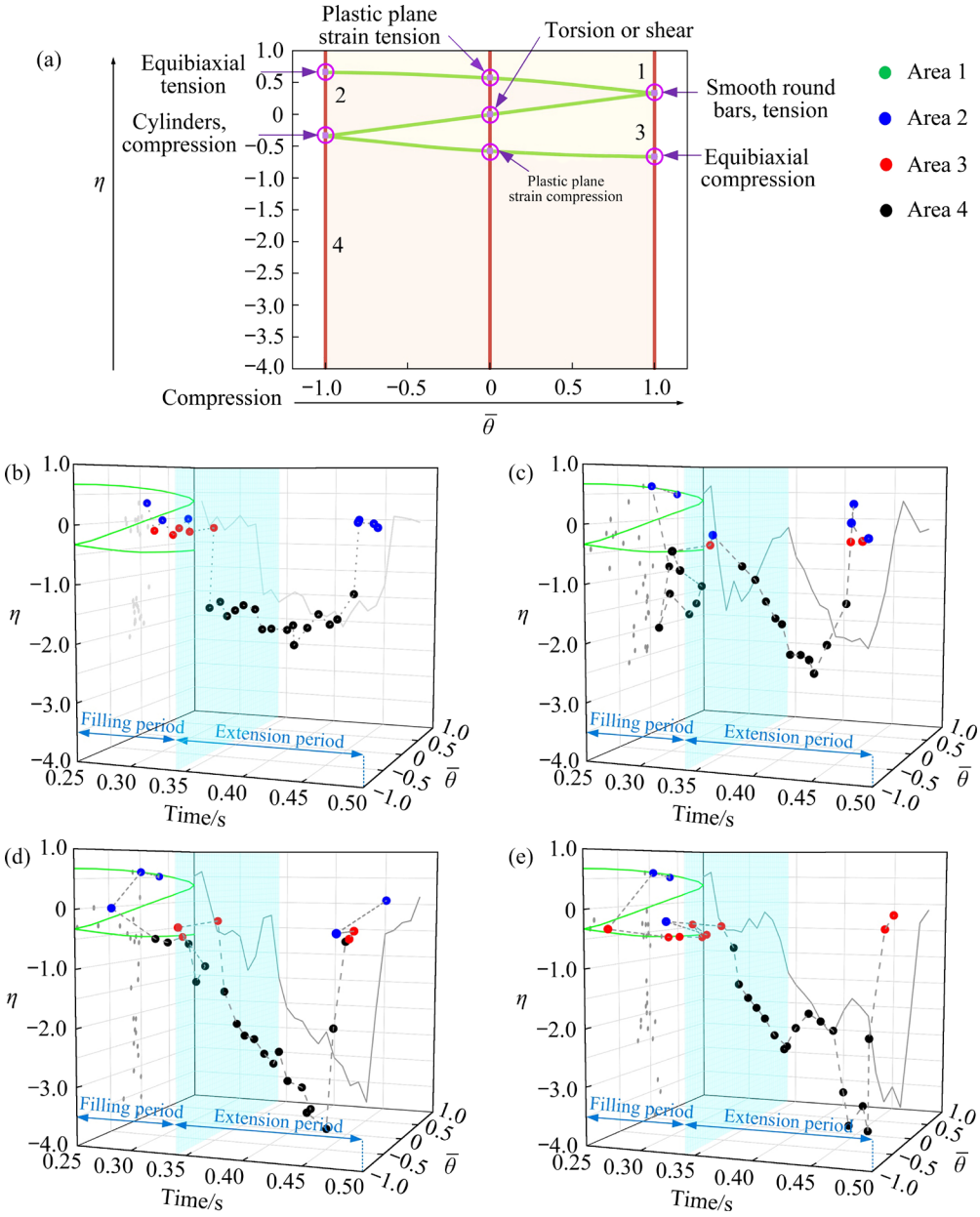

Fig. 8 Stress state at characteristic positions for lower Cu surface: (a) η–$\bar{\theta}$ plane; (b) Front waist; (c) Peak; (d) Back waist; (e) Trough

$\bar{\theta}$ is defined as

$$\bar{\theta}=1-\frac{2}{\pi}\arccos\left(\frac{r}{\bar{\sigma}}\right)^3 \tag{3}$$

where

$$r=\{\frac{27}{2}[(\sigma_1-\sigma_m)(\sigma_2-\sigma_m)(\sigma_3-\sigma_m)+2\tau_{12}\tau_{23}\tau_{31}-(\sigma_1-\sigma_m)\tau_{23}^2-(\sigma_2-\sigma_m)\tau_{31}^2-(\sigma_3-\sigma_m)\tau_{12}^2]\}^{1/3} \tag{4}$$

The range of $\bar{\theta}$ is $-1\leq\bar{\theta}\leq1$.

The distribution of the four characteristic positions from the entrance to the exit in the $\eta-\bar{\theta}$ plane is calculated by Eq. (1) and Eq. (3), as shown in Figs. 8(b−e).

Each characteristic position is distributed in Area 2 when it starts to deform. During the filling period, the front waist bears two tensile and one compressive stresses or two compressive and one tensile stresses, which are distributed in Area 2 and Area 3. The peak changes from two tensile stresses and one compressive stress to triaxial compressive stresses, and it changes to two tensile stresses and one compressive stress at the end of the filling period. This is because the peak is the first to contact the corrugated roller and detaches from the corrugated roller in the subsequent process. The change process of the stress state at the back waist is similar to that at the peak. The stress state of the trough changes from two tensile stresses and one compressive stress to two compressive stresses and one tensile stress, and it becomes two tensile stresses and one compressive stress at the end of the filling period. During the extension period, each characteristic position is mainly subjected to triaxial compressive stresses. At the end of the extension period, the front waist, peak and back waist transform into a stress state of two tensile stresses and one compressive stress. The trough is subjected to two compressive stresses and one tensile stress.

3.5 Microstructure

Figure 9 shows microstructures of characteristic positions on the lower surface of the Cu plate in the original plate and deformation zone (Regions III

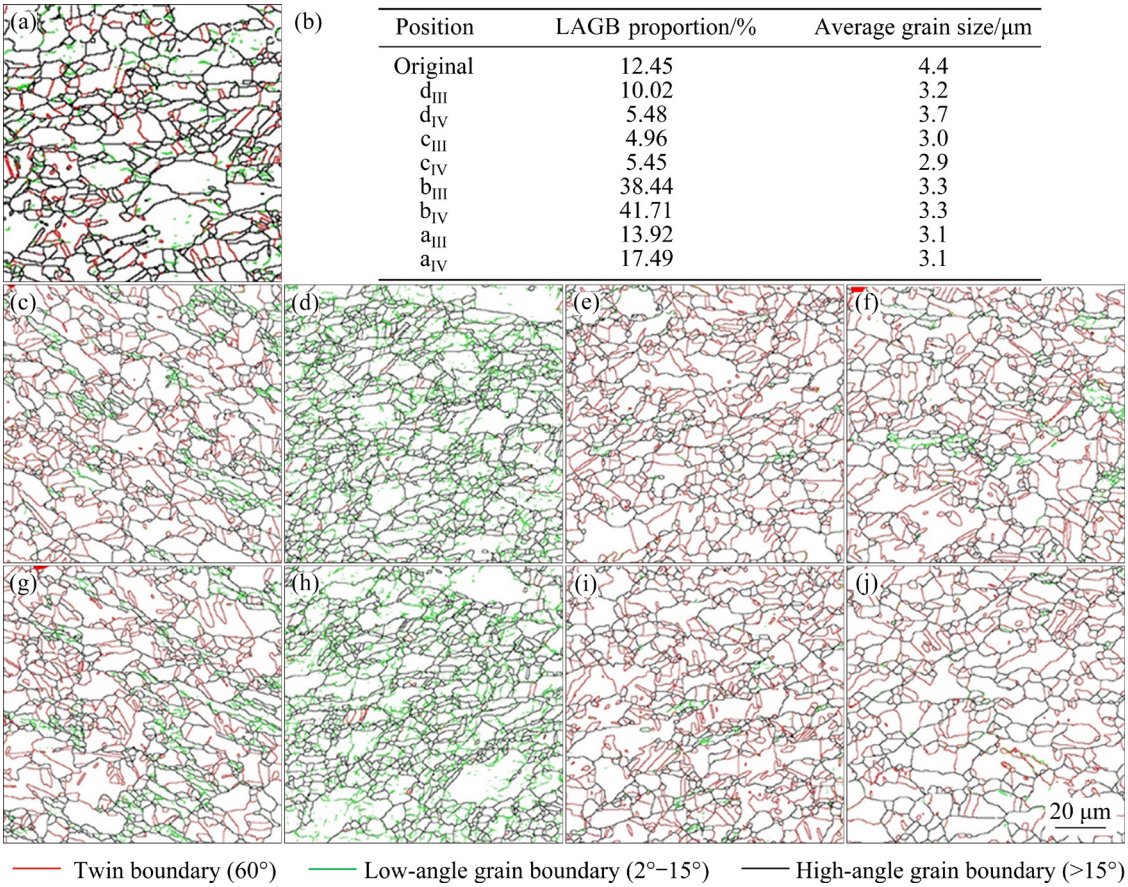

Position	LAGB proportion/%	Average grain size/μm
Original	12.45	4.4
d_{III}	10.02	3.2
d_{IV}	5.48	3.7
c_{III}	4.96	3.0
c_{IV}	5.45	2.9
b_{III}	38.44	3.3
b_{IV}	41.71	3.3
a_{III}	13.92	3.1
a_{IV}	17.49	3.1

Fig. 9 Microstructures of characteristic positions on lower surface of Cu plate: (a) Original plate; (b) Data of characteristic positions; (c−f) a_{III}−d_{III}, respectively; (g−j) a_{IV}−d_{IV}, respectively

and IV). The type of grain boundary is determined by the misorientation angle and is expressed using different colors. Compared with the original plate, the grains at all the characteristic positions in Region III are obviously refined. The average grain size at back waist c_{III} is the smallest, the average grain size at peak b_{III} is the largest, and the grain size at wave trough d_{III} is slightly larger than that at front wave waist a_{III}. Correspondingly, the stress at back waist c_{III} is the largest, and the stress at the peak is the smallest, as shown in Fig. 5(b). Due to the hardening of metal during the deformation process, the position with high stress tends to deform more severely, and the degree of grain refinement is greater [27]. However, the grain size and stress are smaller at front waist a_{III} than those at the trough d_{III} in Region III. The front waist a_{III} undergoes a longer cross shear action (as shown in Fig. 7), which promotes grain refinement. As shown in Figs. 9(b−f), the proportion of low-angle grain boundaries (LAGBs) at peak b_{III} is the largest (38.44%), and the proportion of LAGBs at back waist c_{III} is the lowest (4.96%). The proportion of LAGBs at the trough is slightly lower than that at the front waist a_{III}. The increase in the fraction of LAGBs is conducive to dislocation migration, resulting in a decrease in the material flow stress. However, high-angle grain boundaries (HAGBs) often hinder the movement of dislocations, which causes dislocation entanglement and an increase in strength at the macro level [28,29]. Therefore, the stress at peak b_{III} is the smallest, and the stress at the back waist c_{III} is the largest.

Compared with Region III, the average grain size and the proportion of different grain boundaries at the front waist a_{IV}, peak b_{IV} and back waist c_{IV} change little in Region IV. The grain grows obviously at trough d_{IV}, and LAGBs decrease obviously, which transform into HAGBs. SHRIVASTAVA and TANDON [30] discovered this phenomenon of grain growth during incremental sheet forming. BECK and SPERRY [31] confirmed that the type of strain-induced boundary migration existed without nucleation. This grain growth mode begins at the initial stage of annealing. ZHILYAEV et al [32] also found the phenomenon of grain refinement first and then coarsening during equal-channel angular pressing and considered that the adiabatic temperature increase was the main factor leading to the growth of Cu grains. In this research, the stress at the trough position d_{IV} increases sharply, and a large strain rate is generated, as shown in Figs. 5(b) and (d), resulting in an adiabatic temperature rise. This provides conditions for boundary migration. Therefore, the grain size at the trough changes from 3.2 to 3.7 μm. However, compared to the grain size of the original plate (4.4 μm), the grain size at each characteristic position was significantly refined, which improved the mechanical properties.

4 Conclusions

(1) The deformation of the Cu/Al composite experienced by all metal particles in the corrugated rolling process can be divided into two periods based on the stress characteristics: the filling period when the stress changes are more complicated and the extension period when the stress change trends are approximate.

(2) During extension period, all characteristic positions undergo cross shear action, and the front waist, peak, back waist and trough of the upper and lower surfaces of the Cu plate are relatively unchanged.

(3) In the corrugated rolling process, the grains at each position are significantly refined. However, the adiabatic temperature rise under the conditions of a high strain rate and large strain causes the grain size at the trough to grow after being refined.

Acknowledgments

This study was financially supported by the National Key R&D Program of China (No. 2018YFA0707300), the National Natural Science Foundation of China (Nos. 51904206, 52105390, 51905372, 51805359), the China Postdoctoral Science Foundation (No. 2020M670705), the Natural Science Foundation of Shanxi Province, China (No. 201801D221130), the Major Program of National Natural Science Foundation of China (No. U1710254), and the Scientific and Technological Innovation Programs of Higher Education Institutions in Shanxi Province, China (No. 2019L0258).

References

[1] LIU Bao-xi, AN Qi, YIN Fu-xing, WANG Shuai, CHEN Cui-xin. Interface formation and bonding mechanisms of

hot-rolled stainless steel clad plate [J]. Journal of Materials Science, 2019, 54(17): 11357−11377.

[2] BAKHTIARI A, SHAMSIPUR A, MIRSALEHI S E. Preparation of bimetallic nano-composite by dissimilar friction stir welding of copper to aluminum alloy [J]. Transactions of Nonferrous Metals Society of China, 2021, 31(5): 1363−1380.

[3] LI Xiao-bing, ZU Guo-yin, DING Ming-ming, MU Yong-liang, WANG Ping. Interfacial microstructure and mechanical properties of Cu/Al clad sheet fabricated by asymmetrical roll bonding and annealing [J]. Materials Science and Engineering A, 2011, 529: 485−491.

[4] PARCHURI P, KOTEGAWA S, YAMAMOTO H, ITO K, MORI A, HOKAMOTO K. Benefits of intermediate-layer formation at the interface of Nb/Cu and Ta/Cu explosive clads [J]. Materials & Design, 2019, 166: 1−10.

[5] KELLER C, MOISY F, NGUYEN N, EVE S, DASHTI A, VIEILLE B, GUILLET A, SAUVAGE X, HUG E. Microstructure and mechanical properties characterization of architectured copper aluminum composites manufactured by cold-drawing [J]. Materials Characterization, 2021, 172: 1−12.

[6] GOGHERI M S, KASIRI-ASGARANI M, BAKHSHESHI-RAD H R, GHAYOUR H, RAFIEI M. Mechanical properties, corrosion behavior and biocompatibility of orthopedic pure titanium−magnesium alloy screw prepared by friction welding [J]. Transactions of Nonferrous Metals Society of China, 2020, 30(11): 2952−2966.

[7] HABILA W, AZZEDDINE H, MEHDI B, TIRSATINE K, BAUDIN T, HELBERT A L, BRISSET F, GAUTROT S, MATHON M H, BRADAI D. Investigation of microstructure and texture evolution of a Mg/Al laminated composite elaborated by accumulative roll bonding [J]. Materials Characterization, 2019, 147: 242−252.

[8] CHANG Dong-xu, WANG Ping, ZHAO Ying-ying. Effects of asymmetry and annealing on interfacial microstructure and mechanical properties of Cu/Al laminated composite fabricated by asymmetrical roll bonding [J]. Journal of Alloys and Compounds, 2020, 815: 1−9.

[9] MA Heng-bo, REN Ke-xu, XIAO Xiao, QIU Ran-feng, SHI Hong-xin. Growth characterization of intermetallic compounds at the Cu/Al solid state interface [J]. Materials Research Express, 2019, 6(10): 1−12.

[10] LI Xiao-bing, ZU Guo-yin, WANG Ping. Effect of strain rate on tensile performance of Al/Cu/Al laminated composites produced by asymmetrical roll bonding [J]. Materials Science and Engineering A, 2013, 575: 61−64.

[11] SAVAGE D J, BEYERLEIN I J, MARA N A, VOGEL S C, MCCABE R J, KNEZEVIC M. Microstructure and texture evolution in Mg/Nb layered materials made by accumulative roll bonding [J]. International Journal of Plasticity, 2020, 125: 1−26.

[12] MO Tai-qian, CHEN Ze-jun, LI Bo-xin, WANG Peng-ju, LIU Qing. Tailoring of interface structure and mechanical properties in ARBed 1100/7075 laminated composites by cold rolling [J]. Materials Science and Engineering A, 2019, 755: 97−105.

[13] CHEN D C. An investigation into deformation mechanisms in the rolling of complex sheets with internal defects [J]. Journal of Engineering Manufacture, 2007, 221(7): 1139−1145.

[14] HUANG Qing-xue, ZHANG Jiang, ZHU Lin, JIANG Li, GAO Xiang-yu. Velocity field analysis of bonding interface on cold-rolled copper/aluminum composite plate [J]. Rare Metal Materials and Engineering, 2017, 46(7): 1749−1755.

[15] DYJA H, MRÓZ S, MILENIN A. Theoretical and experimental analysis of the rolling process of bimetallic rods Cu-steel and Cu−Al [J]. Journal of Materials Processing Technology, 2004, 153/154: 100−107.

[16] PAN S C, HUANG M N, TZOU G Y, SYU S W. Analysis of asymmetrical cold and hot bond rolling of unbounded clad sheet under constant shear friction [J]. Journal of Materials Processing Technology, 2006, 177(1/2/3): 114−120.

[17] LU Ri-huan, LIU Yu-tong, MENG Yan, SUN Jing-na, SHEN Liu-feng, HUANG Hua-gui. Theoretical, experimental and numerical studies on the deep drawing behavior of Ti/Al composite sheets with different thickness ratios fabricated by roll bonding [J]. Journal of Materials Processing Technology, 2021, 297: 1−20.

[18] MOHEBBI M S, AKBARZADEH A. Constitutive equation and FEM analysis of incremental cryo-rolling of UFG AA1050 and AA5052 [J]. Journal of Materials Processing Technology, 2018, 255: 35−46.

[19] WANG Tao, LI Sha, REN Zhong-kai, HAN Jian-chao, HUANG Qing-xue. A novel approach for preparing Cu/Al laminated composite based on corrugated roll [J]. Materials Letters, 2019, 234: 79−82.

[20] WANG Tao, WANG Yue-lin, BIAN Li-ping, HUANG Qing-xue. Microstructural evolution and mechanical behavior of Mg/Al laminated composite sheet by novel corrugated rolling and flat rolling [J]. Materials Science and Engineering A, 2019, 765: 1−12.

[21] WANG Tao, LI Sha, NIU Hui, LUO Chao, MA Xiao-bao, LIU Yuan-ming, HAN Jian-chao, BASHIR M U. EBSD research on the interfacial microstructure of the corrugated Mg/Al laminated material [J]. Journal of Materials Research and Technology, 2020, 9(3): 5840−5847.

[22] WANG Tao, LIU Wen-li, LIU Yuan-ming, WANG Zhen-hua, IGNATOV A V, HUANG Qing-xue. Formation mechanism of dynamic multi-neutral points and cross shear zones in corrugated rolling of Cu/Al laminated composite [J]. Journal of Materials Processing Technology, 2021, 295: 1−11.

[23] HUA Fuan, ZHANG Chao-yi, LI Qiang, YU Bao-yi, LIU Wei-hua, LI Run-xia, XIE Shui-sheng, HUANG Guo-jie, CHENG Lei, FU Yao, WANG Hao. Numerical simulation of rolling process and microstructure evolution of AM50 Mg alloy during hot rolling process [J]. Advanced Materials Research, 2011, 291/292/293/294: 449−454.

[24] JI Y H, PARK J J. Development of severe plastic deformation by various asymmetric rolling processes [J]. Materials Science and Engineering A, 2009, 499(1/2): 14−17.

[25] BAI Yuan-li, WIERZBICKI T. A new model of metal plasticity and fracture with pressure and lode dependence [J]. International Journal of Plasticity, 2008, 24(6): 1071−1096.

[26] WANG Zhong-ren. Physical essence of Lode parameter and its effect on plastic flow [J]. Acta Mechanica Solida Since,

2006, 27(3): 277−282.
[27] BALASUNDAR I, RAVI K R, RAGHU T. Grain refinement in OFHC Cu subjected to repetitive upsetting extrusion (RUE) process [J]. Materials Science Forum, 2012, 710: 270−275.
[28] MENG Bao, CAO Bo-nan, WAN Min, WANG Chuan-jie, SHAN De-bin. Constitutive behavior and microstructural evolution in ultrasonic vibration assisted deformation of ultrathin superalloy sheet [J]. International Journal of Mechanical Sciences, 2019, 157/158: 609−618.
[29] YANG D K, HODGSON P D, WEN C E. Simultaneously enhanced strength and ductility of titanium via multimodal grain structure [J]. Scripta Materialia, 2010, 63(9): 941−944.
[30] SHRIVASTAVA P, TANDON P. Microstructure and texture based analysis of forming behavior and deformation mechanism of AA1050 sheet during single point incremental forming [J]. Journal of Materials Processing Technology, 2019, 266: 292−310.
[31] BECK P A, SPERRY P R. Strain induced grain boundary migration in high purity aluminum [J]. Journal of Applied Physics, 1950, 21: 150−152.
[32] ZHILYAEV A P, SWAMINATHAN S, PSHENICHNYUK A I, LANGDON T G, MCNELLEY T R. Adiabatic heating and the saturation of grain refinement during SPD of metals and alloys: Experimental assessment and computer modeling [J]. Journal of Materials Science, 2013, 48(13): 4626−4636.

波纹轧制制备 Cu/Al 复合板的应力分析及显微组织演变

刘延啸[1]，刘元铭[1,2,3]，王振华[1,2,3]，刘燕萍[1]，王 涛[1,2,3]，黄庆学[1,2,3]

1. 太原理工大学 机械与运载工程学院，太原 030024；
2. 太原理工大学 先进金属复合材料成形技术与装备教育部工程研究中心，太原 030024；
3. 太原理工大学 中澳联合研究中心，太原 030024

摘 要：建立三维有限元模型，并通过 50%压下量的轧制试验验证模型的准确性。从时间角度分析整个波纹轧制过程中金属的流动规律。金属经历的变形可以分为两个阶段：填充阶段和压下阶段。填充阶段应力变化较为复杂，而压下阶段应力变化趋势一致。通过罗德参数和应力三轴度分析特征位置的应力状态，在开始变形时为两向拉应力一向压应力。采用 EBSD 技术分析 Cu 板的显微组织演变过程。与原始板材相比，铜板各特征位置晶粒均发生细化，而 Cu 板波谷处晶粒在发生细化后有长大的现象，这是由剧烈塑性变形产生的绝热温升现象造成的。

关键词：Cu/Al 复合板；波纹轧制；变形行为；应力分析；显微组织演变

(Edited by Wei-ping CHEN)